

Bardeen black hole surrounded by perfect fluid dark matter

He-Xu Zhang, Yuan Chen, Tian-Chi Ma, Peng-Zhang He, and Jian-Bo Deng*

Institute of Theoretical Physics & Research Center of Gravitation,

Lanzhou University, Lanzhou 730000, China

Abstract

We derive an exact solution of the spherically symmetric Bardeen black hole surrounded by perfect fluid dark matter (PFDM). By treating the magnetic charge g and dark matter parameter α as thermodynamic variables, we find that the thermodynamic first law and the corresponding Smarr formula are satisfied. The thermodynamic stability of the black hole is also studied. The result show that, there exists a critical radius r_+^C , where the heat capacity diverges, suggesting that the black hole is thermodynamically stable in the range $0 < r_+ < r_+^C$. In addition, the critical radius r_+^C increases with the magnetic charge g and decreases with the dark matter parameter α . Applying the Newman-Janis algorithm, we generalize the spherically symmetric solution to the corresponding rotating black hole. With the metric at hand, the horizons and ergospheres are studied. It turns out that for a fixed dark matter parameter α , in a certain range, with the increase of the rotation parameter a and magnetic charge g , the Cauchy horizon radius increases while the event horizon radius decreases. Finally, we investigate the energy extraction by the Penrose process in rotating Bardeen black hole surrounded by PFDM.

* Jian-Bo Deng: dengjb@lzu.edu.cn

I. INTRODUCTION

The singularity theorems proved by Penrose and Hawking, states that under the main assumptions of the strong energy condition holds and the global hyperbolicity exists, in the frame-work of general relativity, every black hole inevitably contains a singularity [1]. At the space-time singularity, the curvatures, densities go to infinity [1, 2] and the predictive power of physical laws is completely broken down. It is widely believed that the space-time singularities are the reflection of the incompleteness of General Relativity, which can be solved in a quantum theory of gravity. Surprisingly, Bardeen in 1968 [3] obtained a black hole solution without a singularity, which can be interpreted as a gravitationally collapsed magnetic monopole arising in a specific form of nonlinear electrodynamics [4]. After that, more regular (non-singular) black holes such as Ayón-Beato and García black hole [5], Hayward black hole [6], and Berej–Matyjasek–Trynieki–Wornowicz black hole [7] were proposed. The spherically symmetric Bardeen black hole is described by the metric

$$ds^2 = -f(r) dt^2 + f(r)^{-1} dr^2 + r^2 d\Omega^2, \quad f(r) = 1 - \frac{2Mr^2}{(r^2 + g^2)^{\frac{3}{2}}}, \quad (1)$$

where g and M are the magnetic charge and mass, respectively. It should be noted that, the metric behaves like the Schwarzschild metric at the large distances ($g/r \ll 1$) and near the origin it behaves like de Sitter geometry, which can be realized from

$$f(r) \simeq 1 - \frac{2M}{g^3} r^2, \quad \frac{g}{r} \gg 1. \quad (2)$$

Eq. (2) suggests that the Bardeen black hole avoids singularities by a de Sitter core, i.e. the pressure is negative and thus would prevent a singular end-state of the gravitationally collapsed matter [8, 9]. It is worth noting that all regular black holes (including Bardeen black holes) violate the weak energy condition, however, the region of violation is always shielded by the Cauchy horizon [10–13]. In fact, this

violation of classical energy conditions is a natural consequence of the fact that the singularity-free metric might incorporate some quantum gravity effects [12].

Modern cosmological observations reveal that our current universe contains mainly of 4.9% baryon matter, 26.8% dark matter, and 68.3% dark energy, according to the Standard Model of Cosmology [14]. Therefore, it is necessary to consider the black hole solutions surrounded by dark matter or dark energy. In recent years, the black hole surrounded by quintessence dark energy have attracted much attention. For example, Kiselev [15] considered the Schwarzschild black hole surrounded by the quintessential energy and then Toshmatov and Stuchlík [16] extended it to the Kerr-like black hole; the quasinormal modes, thermodynamics and phase transition from Bardeen Black hole surrounded by quintessence was discussed by Saleh and Thomas [17]; the Hayward black holes surrounded by quintessence have been studied in Ref. [18], etc [19–24]. On the other hand, as one of the dark matter candidates, the perfect fluid dark matter has been proposed by Kiselev [15, 25] and further studied in Ref. [26], which offers a reasonable explanation for the asymptotically flat rotating velocity in spiral galaxies, see Refs. [27–31] for more recent researches. In this work, following Refs. [16, 18], we generalize the Schwarzschild black hole surrounded by PFDM to the spherically symmetric Bardeen black hole. Furthermore, by resorting to the Newman-Janis algorithm we obtain the rotating Bardeen black hole in PFDM.

The paper is organized as follows. The next section is the derivation of the spherically symmetric Bardeen black hole surrounded by perfect fluid dark matter. In Sec. III, we discuss its thermodynamic properties. In Sec. IV, by applying the Newman-Janis algorithm we obtain the rotating Bardeen black hole surrounded by perfect fluid dark matter. The weak energy condition is the subject of Sec. V. In Sec. VI, the horizons and the ergospheres of Bardeen black hole surrounded by perfect fluid dark matter have been studied. In Sec. VII, we investigate the energy extraction by the Penrose process. Conclusions and discussions are presented in

Sec. VIII. Planck units $\hbar = G = c = k_B = 1$ are used throughout the paper.

II. STATIC AND SPHERICALLY SYMMETRIC BARDEEN BLACK HOLE IN PERFECT FLUID DARK MATTER

Given the coupling between gravitational and a non-linear electromagnetic field, the Einstein-Maxwell equations should be modified as

$$G_{\mu}^{\nu} = 2 \left(\frac{\partial \mathcal{L}(F)}{\partial F} F_{\mu\lambda} F^{\nu\lambda} - \delta_{\mu}^{\nu} \mathcal{L} \right) + 8\pi T_{\mu}^{\nu}, \quad (3)$$

$$\nabla_{\mu} \left(\frac{\partial \mathcal{L}(F)}{\partial F} F^{\nu\mu} \right) = 0, \quad (4)$$

$$\nabla_{\mu} (*F^{\nu\mu}) = 0. \quad (5)$$

Here, $F_{\mu\nu} = 2\nabla_{[\mu} A_{\nu]}$ and \mathcal{L} is a function of $F \equiv \frac{1}{4} F_{\mu\nu} F^{\mu\nu}$ given by [4]

$$\mathcal{L}(F) = \frac{3M}{|g|^3} \left(\frac{\sqrt{2g^2 F}}{1 + \sqrt{2g^2 F}} \right)^{\frac{5}{2}}, \quad (6)$$

where g and M are the parameters associated with magnetic charge and mass, respectively.

In this work, we consider the black holes surrounded by the perfect fluid dark matter. Following Kiselev [15, 25] and Li and Yang [26], the energy-momentum tensor of PFDM in the standard orthogonal basis is given by $T_{\nu}^{\mu} = \text{diag}(-\epsilon, p_r, p_{\theta}, p_{\phi})$, with the density, radial and tangential pressures of the PFDM

$$-\epsilon = p_r = \frac{\alpha}{8\pi r^3} \quad \text{and} \quad p_{\theta} = p_{\phi} = -\frac{\alpha}{16\pi r^3}. \quad (7)$$

To obtain a solution satisfies Eqs. (3)-(5), we assume a spherically symmetric line element

$$ds^2 = -f(r) dt^2 + f(r)^{-1} dr^2 + r^2 d\Omega^2, \quad f(r) = 1 - \frac{2m(r)}{r}, \quad (8)$$

and use the ansatz for Maxwell field [4]

$$F_{\mu\nu} = (\delta_\mu^\theta \delta_\nu^\varphi - \delta_\nu^\theta \delta_\mu^\varphi) B(r, \theta). \quad (9)$$

Next, using Eqs. (4) and (5), Eq. (9) can be simplified as

$$F_{\mu\nu} = (\delta_\mu^\theta \delta_\nu^\varphi - \delta_\nu^\theta \delta_\mu^\varphi) g \sin \theta, \quad (10)$$

where g is the integration constant. Further, one can get $F = g^2/2r^4$. In order to give a direct physical interpretation to g , for any 2-sphere S at infinity, we consider the following integral

$$\frac{1}{4\pi} \int_S *F = \frac{g}{4\pi} \int_0^\pi \int_0^{2\pi} \sin \theta d\theta d\varphi = g. \quad (11)$$

From Eq. (11), one can confirm that g is the magnetic monopole charge.

Now, with the help of the above equations, the time component of Eq. (3) reduces to

$$-\frac{2}{r^2} \frac{dm(r)}{dr} = -\frac{6Mg^2}{(r^2 + g^2)^{\frac{5}{2}}} + \frac{\alpha}{r^3}. \quad (12)$$

Integrating Eq. (12) from r to ∞ and using that $M = \lim_{r \rightarrow \infty} \left(m(r) + \frac{\alpha}{2} \ln \frac{r}{|\alpha|} \right)$, one finally gets

$$f(r) = 1 - \frac{2Mr^2}{(r^2 + g^2)^{\frac{3}{2}}} + \frac{\alpha}{r} \ln \frac{r}{|\alpha|}. \quad (13)$$

Note that, in the absence of PFDM, i.e. $\alpha = 0$, the above space-time recovers that of the Bardeen black hole; in the case of $g = 0$ [3, 4], it reduces to the Schwarzschild black hole surrounded by PFDM [25, 26]; if $\alpha = 0$ and $g = 0$, we will obtain the Schwarzschild black hole.

As was mentioned in the introduction, the Bardeen black hole ($\alpha = 0$) is regular everywhere. To check whether this character is changed by the presence of perfect

fluid dark matter, we calculate the following curvature scalars

$$R = \frac{6Mg^2(4g^2 - r^2)}{(g^2 + r^2)^{\frac{7}{2}}} - \frac{\alpha}{r^3}, \quad (14)$$

$$R_{\mu\nu}R^{\mu\nu} = \frac{18M^2g^4(8g^4 - 4g^2r^2 + 13r^4)}{(g^2 + r^2)^7} - \frac{6Mg^2(2g^2 + 7r^2)\alpha}{r^3(g^2 + r^2)^{\frac{7}{2}}} + \frac{5\alpha^2}{2r^6}, \quad (15)$$

$$\begin{aligned} \mathcal{K} = R_{\mu\nu\sigma\tau}R^{\mu\nu\sigma\tau} &= \frac{12\alpha^2 \ln^2 \frac{r}{|\alpha|}}{r^6} + \frac{13\alpha^2}{r^6} + \frac{4\alpha \ln \frac{r}{|\alpha|} \left[\frac{6Mr^5(3g^2 - 2r^2)}{(g^2 + r^2)^{7/2}} - 5\alpha \right]}{r^6} \\ &+ \frac{4\alpha M(-2g^4 - 37g^2r^2 + 10r^4)}{r^3(g^2 + r^2)^{7/2}} + \frac{12M^2(8g^8 - 4g^6r^2 + 47g^4r^4 - 12g^2r^6 + 4r^8)}{(g^2 + r^2)^7}. \end{aligned} \quad (16)$$

It turns out that the Bardeen black hole surrounded by PFDM is singular at $r = 0$; in fact, the future singularity comes from the dark matter background.

III. THERMODYNAMIC PROPERTIES OF BARDEEN BLACK HOLE IN PFDM

Let us now turn to the thermodynamic properties of the Bardeen black hole in perfect fluid dark matter. For convenience, we write here the line element of spherically symmetric black hole obtained in the previous section as

$$\begin{aligned} ds^2 &= -f(r) dt^2 + f(r)^{-1} dr^2 + r^2 d\Omega^2, \\ f(r) &= 1 - \frac{2Mr^2}{(r^2 + g^2)^{\frac{3}{2}}} + \frac{\alpha}{r} \ln \frac{r}{|\alpha|}. \end{aligned} \quad (17)$$

The black hole mass M can be expressed in terms of event horizon r_+ as

$$M = \frac{(r_+^2 + g^2)^{\frac{3}{2}}}{2r_+^2} \left(1 + \frac{\alpha}{r_+} \ln \frac{r_+}{|\alpha|} \right), \quad (18)$$

which comes from $f(r_+) = 0$. According to the Bekenstein area law, the entropy S of black hole can be calculated as

$$S = \frac{\mathcal{A}}{4} = \int_0^{2\pi} \int_0^\pi \sqrt{g_{\theta\theta}g_{\varphi\varphi}} d\theta d\varphi = \pi r_+^2. \quad (19)$$

Making use of it, one can rewrite Eq. (18) as

$$M = \frac{(S + \pi g^2)^{\frac{3}{2}}}{2\sqrt{\pi}S} \left(1 + \frac{\sqrt{\pi}\alpha}{\sqrt{S}} \ln \frac{\sqrt{S}}{\sqrt{\pi}|\alpha|} \right). \quad (20)$$

Other thermodynamic quantities can be obtained through thermodynamic identities. For examples, the temperature T , the magnetic potential Ψ and the conjugate quantity to the dark matter parameter α are given by

$$T = \left(\frac{\partial M}{\partial S} \right)_{g,\alpha} = \frac{\sqrt{r_+^2 + g^2} \left(r_+ (r_+^2 - 2g^2) + \alpha (r_+^2 + g^2) - 3g^2 \alpha \ln \frac{r_+}{|\alpha|} \right)}{4\pi r_+^5}, \quad (21)$$

$$\Psi = \left(\frac{\partial M}{\partial g} \right)_{T,\alpha} = \frac{3g\sqrt{r_+^2 + g^2} \left(r_+ + \alpha \ln \frac{r_+}{|\alpha|} \right)}{2r_+^3}, \quad (22)$$

$$\Pi = \left(\frac{\partial M}{\partial \alpha} \right)_{T,g} = \frac{(r_+^2 + g^2)^{\frac{3}{2}} \left(-1 + \ln \frac{r_+}{|\alpha|} \right)}{2r_+^3}. \quad (23)$$

Note that here we have treated the dark matter parameter α as a new thermodynamic variable and Π is its conjugate quantity, as shown in Refs. [32–35]. It is easy to check that those thermodynamic quantities satisfy the first law of black hole thermodynamics

$$dM = TdS + \Psi dg + \Pi d\alpha, \quad (24)$$

and the Smarr formula

$$M = 2TS + \Psi g + \Pi \alpha, \quad (25)$$

which is exactly consistent with the scaling dimensional argument.

In what follows, we will investigate the thermodynamic stability of the Bardeen black hole in perfect fluid dark matter. The heat capacity at constant volume is defined as

$$C_V = T \frac{\partial S}{\partial T} = T \frac{\partial S}{\partial r_+} \left(\frac{\partial T}{\partial r_+} \right)^{-1}. \quad (26)$$

Plugging Eqs. (19) and (21) into (26), one finally arrives at

$$C_V = -\frac{2\pi r_+^2 (r_+^2 + g^2) \left(r_+^3 + \alpha r_+^2 - 2g^2 r_+ + g^2 \alpha - 3g^2 \alpha \ln \frac{r_+}{|\alpha|} \right)}{r_+^4 (r_+ + 2\alpha) - 8g^4 (r_+ - \alpha) + 2g^2 r_+^2 (5\alpha - 2r_+) - 3g^2 (5g^2 + 4r_+^2) \alpha \ln \frac{r_+}{|\alpha|}}. \quad (27)$$

The behavior of C_V against r_+ was plotted in Fig. 1 for different values of the magnetic charge g and the dark matter parameter α . As we can see, for given values of parameters a and g , there is a critical radius r_+^C where heat capacity C_V diverge and the second order phase transition occurs. The Fig. 1 indicates the heat capacity is positive and the black hole is thermodynamically stable in the range $0 < r_+ < r_+^C$. Clearly, one can find that the critical radius r_+^C increases with the magnetic charge g and decreases with the dark matter parameter α .

IV. ROTATING BARDEEN BLACK HOLE IN PERFECT FLUID DARK MATTER

In this section, with the Newman-Janis algorithm (NJA), we will generalize the spherically symmetric Bardeen black hole solution in perfect fluid dark matter to Kerr-like rotational black hole solution. The NJA was first proposed by Newman and Janis in 1965 [36] and widely used in many articles [16, 18, 37–45]. In this work, we will adopt the NJA modified by Azreg-Ainou [46, 47], which can generate rotating regular black hole solutions without complexification.

Consider the general static and spherically symmetric metric:

$$ds^2 = -f(r) dt^2 + g(r)^{-1} dr^2 + h(r) d\Omega^2, \quad d\Omega^2 = d\theta^2 + \sin^2 \theta d\varphi^2. \quad (28)$$

At the first step of this algorithm, we transform the spherically symmetric space-time metric (28) from the Boyer-Lindquist (BL) coordinates (t, r, θ, φ) to the Eddington-Finkelstein (EF) coordinates (u, r, θ, φ) by carrying out the coordinate transforma-

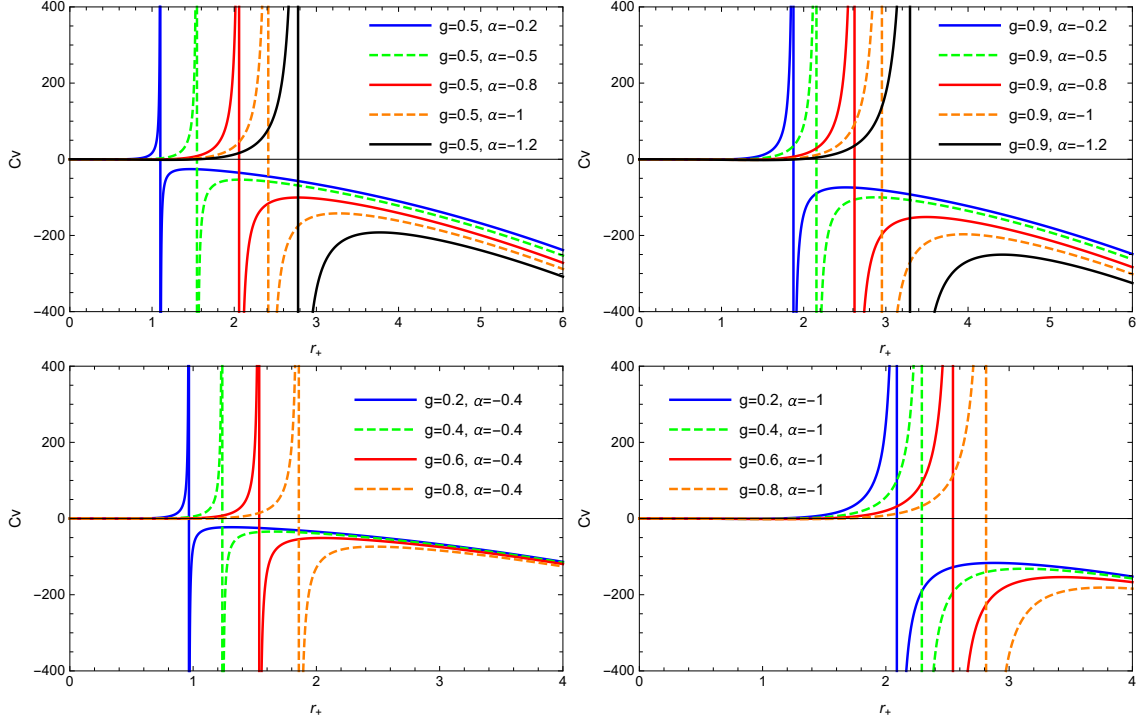


Figure 1: Variation of heat capacity with respect to the event horizon r_+ for a set of values of parameters g and α .

tion

$$du = dt - \frac{dr}{\sqrt{f(r)g(r)}}. \quad (29)$$

As the result of this transformation, the line element (28) takes the form

$$ds^2 = -f(r) du^2 - 2\sqrt{\frac{f(r)}{g(r)}} du dr + h(r) (d\theta^2 + \sin^2 \theta d\varphi^2). \quad (30)$$

In terms of the null tetrads satisfy the relations $l_\mu l^\mu = n_\mu n^\mu = m_\mu m^\mu = l_\mu m^\mu = n_\mu m^\mu = 0, l_\mu n^\mu = -m_\mu \bar{m}^\mu = 1$, the contravariant metric tensor associated with the line element (30) can be expressed as

$$g^{\mu\nu} = -l^\mu n^\nu - l^\nu n^\mu + m^\mu \bar{m}^\nu + m^\nu \bar{m}^\mu, \quad (31)$$

where

$$\begin{aligned}
l^\mu &= \delta_r^\mu, & n^\mu &= \sqrt{\frac{g(r)}{f(r)}} \delta_0^\mu - \frac{f(r)}{2} \delta_r^\mu, \\
m^\mu &= \frac{1}{\sqrt{2h(r)}} \delta_\theta^\mu + \frac{i}{\sqrt{2h(r)} \sin \theta} \delta_\varphi^\mu, & \bar{m}^\mu &= \frac{1}{\sqrt{2h(r)}} \delta_\theta^\mu - \frac{i}{\sqrt{2h(r)} \sin \theta} \delta_\varphi^\mu.
\end{aligned} \tag{32}$$

Next, we take the critical step of the NJA, which is to perform complex coordinate transformations in the $u - r$ plane

$$\begin{aligned}
u &\rightarrow u - ia \cos \theta, \\
r &\rightarrow r + ia \cos \theta.
\end{aligned} \tag{33}$$

At the same time, we assume that as the result of these transformations the metric functions also turn into a new form: $f(r) \rightarrow F(r, a, \theta)$, $g(r) \rightarrow G(r, a, \theta)$, and $h(r) \rightarrow \Sigma = r^2 + a^2 \cos^2 \theta$ [46, 47]. Furthermore, null tetrads also take the new form

$$\begin{aligned}
l^\mu &= \delta_r^\mu, & n^\mu &= \sqrt{\frac{G}{F}} \delta_0^\mu - \frac{1}{2} F \delta_r^\mu, \\
m^\mu &= \frac{1}{\sqrt{2\Sigma}} \left(\delta_\theta^\mu + ia \sin \theta (\delta_0^\mu - \delta_r^\mu) + \frac{i}{\sin \theta} \delta_\varphi^\mu \right), \\
\bar{m}^\mu &= \frac{1}{\sqrt{2\Sigma}} \left(\delta_\theta^\mu - ia \sin \theta (\delta_0^\mu - \delta_r^\mu) - \frac{i}{\sin \theta} \delta_\varphi^\mu \right).
\end{aligned} \tag{34}$$

Then by means of Eq. (31), the contravariant components of the metric $g^{\mu\nu}$ can be obtained as

$$\begin{aligned}
g^{uu} &= \frac{a^2 \sin^2 \theta}{\Sigma}, & g^{rr} &= G + \frac{a^2 \sin^2 \theta}{\Sigma}, \\
g^{\theta\theta} &= \frac{1}{\Sigma}, & g^{\varphi\varphi} &= \frac{1}{\Sigma \sin^2 \theta}, \\
g^{ur} &= g^{ru} = -\sqrt{\frac{G}{F}} - \frac{a^2 \sin^2 \theta}{\Sigma}, \\
g^{u\varphi} &= g^{\varphi u} = \frac{a}{\Sigma}, & g^{r\varphi} &= g^{\varphi r} = -\frac{a}{\Sigma}.
\end{aligned} \tag{35}$$

Accordingly, the rotating metric in the EF coordinates of (u, r, θ, φ) reads

$$\begin{aligned} ds^2 = & -F du^2 - 2\sqrt{\frac{F}{G}} du dr + 2a \left(F - \sqrt{\frac{F}{G}} \right) \sin^2 \theta du d\varphi + \Sigma d\theta^2 \\ & + 2a \sin^2 \theta \sqrt{\frac{F}{G}} dr d\varphi + \sin^2 \theta \left[\Sigma + a^2 \left(2\sqrt{\frac{F}{G}} - F \right) \sin^2 \theta \right] d\varphi^2. \end{aligned} \quad (36)$$

The last step of NJA is to bring (36) to the BL coordinates by using the following coordinate transformations:

$$du = dt + \lambda(r) dr, \quad d\varphi = d\phi + \chi(r) dr, \quad (37)$$

where the functions $\lambda(r)$ and $\chi(r)$ can be found using the requirement that all the nondiagonal components of the metric tensor, except the coefficient $g_{t\phi}$ ($g_{\phi t}$), are equal to zero [46, 47]. Thus,

$$\lambda(r) = -\frac{k(r) + a^2}{g(r)h(r) + a^2}, \quad \chi(r) = -\frac{a}{g(r)h(r) + a^2}, \quad (38)$$

with

$$k(r) = \sqrt{\frac{g(r)}{f(r)}} h(r), \quad (39)$$

and

$$F(r, \theta) = \frac{(gh + a^2 \cos^2 \theta) \Sigma}{(k^2 + a^2 \cos^2 \theta)^2}, \quad G(r, \theta) = \frac{gh + a^2 \cos^2 \theta}{\Sigma}. \quad (40)$$

Here, for convenience, we omit the variables of $f(r)$, $g(r)$, $h(r)$ and $k(r)$.

Finally, the rotating solution corresponding to the spherically symmetric metric (28) can therefore be obtained as

$$\begin{aligned} ds^2 = & -\frac{(gh + a^2 \cos^2 \theta) \Sigma}{(k + a^2 \cos^2 \theta)^2} dt^2 + \frac{\Sigma}{gh + a^2} dr^2 - 2a \sin^2 \theta \left[\frac{k - gh}{(k + a^2 \cos^2 \theta)^2} \right] \Sigma d\phi dt \\ & + \Sigma d\theta^2 + \Sigma \sin^2 \theta \left[1 + a^2 \sin^2 \theta \frac{2k - gh + a^2 \cos^2 \theta}{(k + a^2 \cos^2 \theta)^2} \right] d\phi^2. \end{aligned} \quad (41)$$

In the case of Bardeen black holes in PFDM, comparing the line elements (17) with (28), one can find

$$f(r) = g(r) = 1 - \frac{2Mr^2}{(r^2 + g^2)^{\frac{3}{2}}} + \frac{\alpha}{r} \ln \frac{r}{|\alpha|}, \quad h(r) = k(r) = r^2. \quad (42)$$

Substituting the above expressions into (41), we therefore obtain the metric of rotating Bardeen black holes in perfect fluid dark matter in the form

$$\begin{aligned} ds^2 = & - \left(1 - \frac{2\rho r}{\Sigma}\right) dt^2 + \frac{\Sigma}{\Delta_r} dr^2 + \Sigma d\theta^2 - \frac{4a\rho r \sin^2 \theta}{\Sigma} dt d\phi \\ & + \sin^2 \theta \left(r^2 + a^2 + \frac{2a^2 \rho r \sin^2 \theta}{\Sigma}\right) d\phi^2, \end{aligned} \quad (43)$$

with

$$\begin{aligned} 2\rho &= \frac{2Mr^3}{(r^2 + g^2)^{\frac{3}{2}}} - \alpha \ln \frac{r}{|\alpha|}, \\ \Sigma &= r^2 + a^2 \cos^2 \theta, \\ \Delta_r &= r^2 + a^2 - \frac{2Mr^4}{(r^2 + g^2)^{\frac{3}{2}}} + \alpha r \ln \frac{r}{|\alpha|}. \end{aligned} \quad (44)$$

Now, we come to consider the energy-momentum tensor in the following. With the help of *Mathematica* package, from the metric (43), the nonvanishing components of the Einstein tensor $G_{\mu\nu}$ are given by

$$\begin{aligned} G_{tt} &= \frac{2(r^4 + a^2 r^2 - 2r^3 \rho - a^4 \sin^2 \theta \cos^2 \theta) \rho'}{\Sigma^3} - \frac{a^2 r \sin^2 \theta \rho''}{\Sigma^2}, \\ G_{t\phi} &= \frac{2a \sin^2 \theta [(r^2 + a^2)(a^2 \cos^2 \theta - r^2) + 2r^3 \rho] \rho'}{\Sigma^3} \\ &\quad + \frac{ar \sin^2 \theta (r^2 + a^2) \rho''}{\Sigma^2}, \\ G_{rr} &= -\frac{2r^2 \rho'}{\Sigma \Delta_r}, \quad G_{\theta\theta} = -\frac{2a^2 \cos^2 \theta \rho'}{\Sigma} - r \rho'', \\ G_{\phi\phi} &= -\frac{a^2 \sin^2 \theta (r^2 + a^2) [a^2 + (2r^2 + a^2) \cos 2\theta]}{\Sigma^3} - \frac{4a^2 r^3 \sin^4 \theta \rho \rho'}{\Sigma^3} - \frac{r \sin^2 \theta (a^2 + r^2)^2 \rho''}{\Sigma^2}, \end{aligned} \quad (45)$$

in which the prime ' denotes the derivative with respect to r .

In order to obtain the components of the energy-momentum tensor, as shown in Refs. [16, 18], we introduce the standard orthonormal basis of the rotating Bardeen black hole in perfect fluid dark matter

$$\begin{aligned}
e_{(t)}^\mu &= \frac{1}{\sqrt{\Delta_r \Sigma}} (r^2 + a^2, 0, 0, a), \\
e_{(r)}^\mu &= \sqrt{\frac{\Delta_r}{\Sigma}} (0, 1, 0, 0), \\
e_{(\theta)}^\mu &= \frac{1}{\sqrt{\Sigma}} (0, 0, 1, 0), \\
e_{(\phi)}^\mu &= -\frac{1}{\sqrt{\Sigma \sin^2 \theta}} (a \sin^2 \theta, 0, 0, 1).
\end{aligned} \tag{46}$$

Combining (45), (46), and the Einstein field equation $G_{\mu\nu} = 8\pi T_{\mu\nu}$, the components of the energy-momentum tensor can be obtained as

$$\begin{aligned}
\epsilon = -p_r = T_{(t)(t)} &= \frac{1}{8\pi} e_{(t)}^\mu e_{(t)}^\nu G_{\mu\nu} = \frac{1}{4\pi} \frac{r^2 \rho'}{\Sigma^2}, \\
p_\theta = p_\phi = T_{(\theta)(\theta)} &= \frac{1}{8\pi} e_{(\theta)}^\mu e_{(\theta)}^\nu G_{\mu\nu} = \epsilon - \frac{2\rho' + r\rho''}{8\pi\Sigma}.
\end{aligned} \tag{47}$$

From Eq. (47), it is easy to find that ϵ , p_r , p_θ , and p_ϕ all contain two contributions: a nonlinear magnetic-charged part and the PFDM.

V. WEAK ENERGY CONDITION

The weak energy condition states that for all physically reasonable classical matter, as measured by any observer in space-time, must be nonnegative [48], i.e.,

$$T_{\mu\nu} \xi^\mu \xi^\nu \geq 0,$$

for all timelike ξ^μ . With the decomposition of the energy-momentum tensor $T_{\mu\nu}$, the weak energy condition is equivalent to

$$\epsilon \geq 0, \quad \epsilon + p_i \geq 0. \tag{48}$$

Substituting Eqs. (44) and (47) into Eq. (48) leads to

$$\epsilon = \frac{1}{4\pi} \frac{r^2}{\Sigma^2} \left[\frac{3g^2 Mr^2}{(r^2 + g^2)^{\frac{5}{2}}} - \frac{\alpha}{2r} \right] \geq 0, \quad (49)$$

$$\epsilon + p_r = 0, \quad (50)$$

$$\epsilon + p_\theta = \epsilon + p_\phi = \frac{2(r^2 - a^2 \cos^2 \theta) \rho' - r \Sigma \rho''}{8\pi \Sigma^2} \geq 0. \quad (51)$$

According to Eq. (47), as examples, we depict the variations of ϵ and $\epsilon + p_\theta / \epsilon + p_\phi$ with r and $\cos \theta$ under two sets of parameters in Figs. 2 and 3. It turns out that the weak energy condition is violated near the origin of the rotating Bardeen in the PFDM, which happens for all the rotating regular black holes [10–13]. In fact, one can realize this by considering the asymptotic behavior of the matter density ϵ and $\epsilon + p_\theta$ near the origin:

$$\epsilon \simeq \frac{6Mr^4 - \alpha g^3 r}{8\pi g^3 (r^2 + a^2)^2} \simeq -\frac{\alpha r}{8\pi (r^2 + a^2)^2}, \quad r \rightarrow 0, \quad (52)$$

$$\epsilon + p_\theta \simeq -\frac{3a^2 Mr^2}{2\pi g^3 (r^2 + a^2)^2} + \frac{\alpha a^2}{16\pi r (r^2 + a^2)^2} \simeq \frac{\alpha}{16\pi a^2 r}, \quad r \rightarrow 0, \quad (53)$$

where we set $\cos \theta = \pm 1$. Eq. (53) implies that, for the rotating Bardeen black hole ($\alpha = 0$), the violation of weak energy cannot be prevented if $a \neq 0$. As a verification of Eqs. (52) and (53), the dependence of ϵ and $\epsilon + p_\theta$ on a and α is plotted in Fig. 4. Further more, at large r , the matter density ϵ and $\epsilon + p_\theta$ behave as

$$\epsilon \simeq \frac{3g^2 M}{4\pi r (r^2 + a^2)^2} - \frac{\alpha r}{8\pi (r^2 + a^2)^2} \simeq -\frac{\alpha}{8\pi r^3}, \quad r \rightarrow \infty, \quad (54)$$

$$\epsilon + p_\theta \simeq \frac{15Mg^2}{8\pi r^5} - \frac{3\alpha}{16\pi r^3} \simeq -\frac{3\alpha}{16\pi r^3}, \quad r \rightarrow \infty \quad (55)$$

for $\cos \theta = \pm 1$. From Eqs. (54) and (55), one can find that for the Bardeen black hole in PFDM, if $\alpha > 0$, then both ϵ and $\epsilon + p_\theta$ are negative at the large distances, which is quite unreasonable from the perspective of observation. Therefore, we always assume $\alpha < 0$ in the following discussions.

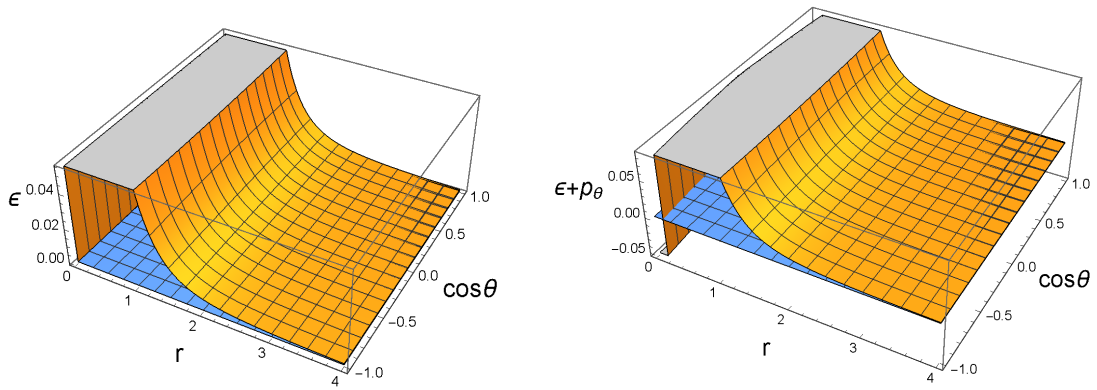


Figure 2: Dependence of matter density ϵ and $\epsilon + p_\theta$ on radius and angle for a rotating Bardeen BH in PFDM with $M = 1, a = 0.2, g = 0.5, \alpha = -1$.

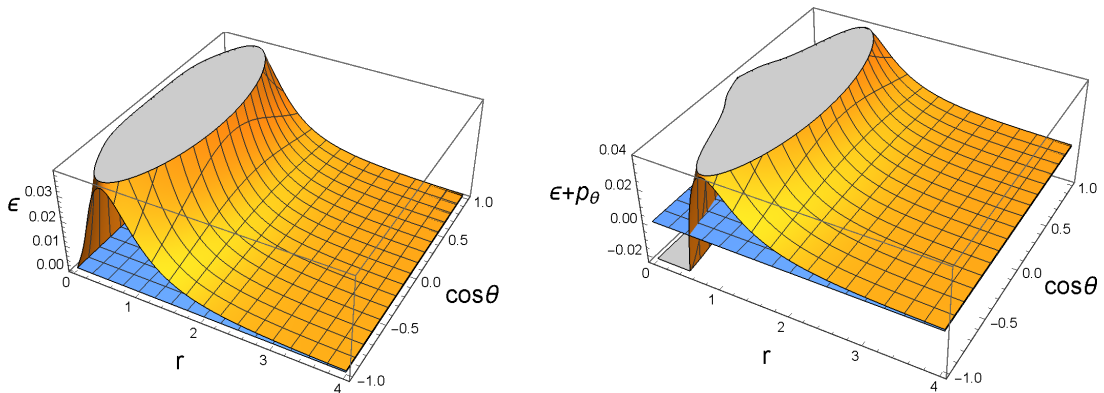


Figure 3: Dependence of matter density ϵ and $\epsilon + p_\theta$ on radius and angle for a rotating Bardeen BH in PFDM with $M = 1, a = 0.9, g = 0.5, \alpha = -1$.

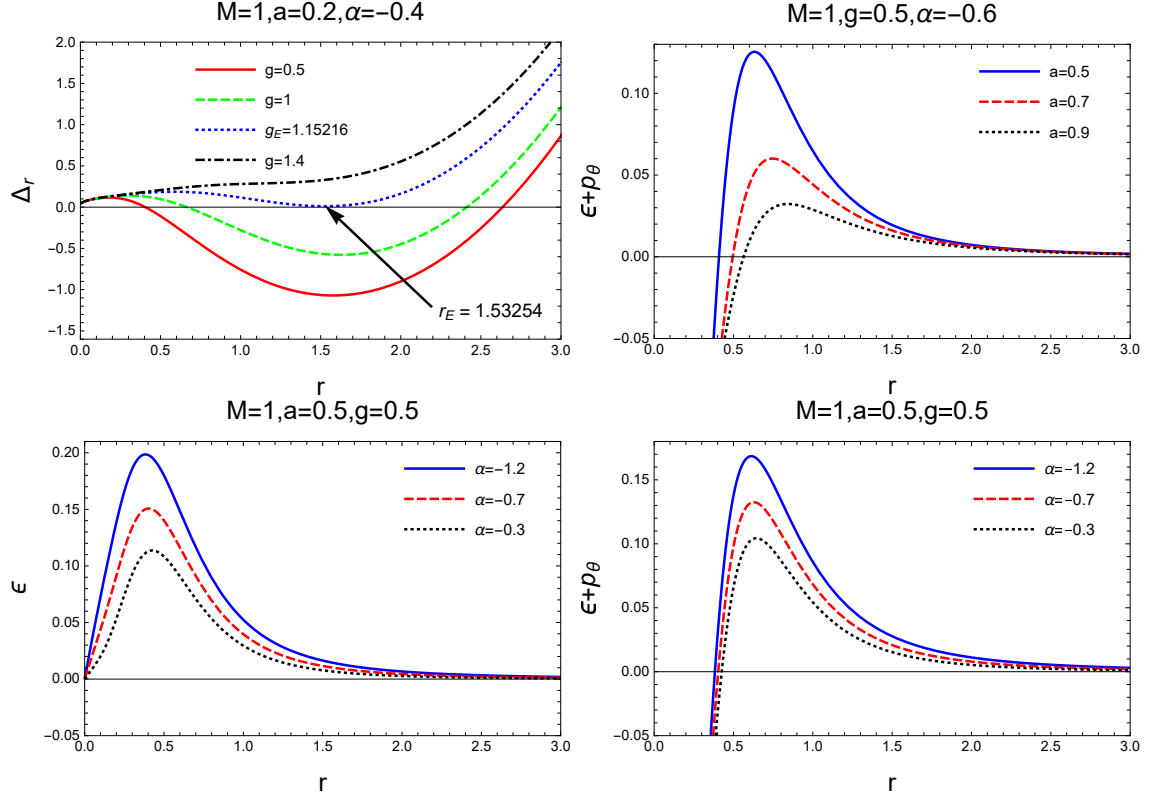


Figure 4: Plot showing ϵ and $\epsilon + p_\theta$ vs. r for various black hole parameters.

VI. PROPERTIES OF ROTATING BARDEEN BLACK HOLE IN PERFECT FLUID DARK MATTER

A. Horizons

Similar to the Kerr black hole, the space-time metric (43) is singular at $\Delta_r = 0$, which corresponds to the horizons of the rotating black hole. In other words, the horizons of the rotating Bardeen black hole in PFDM are solutions of

$$\Delta_r = r^2 + a^2 - \frac{2Mr^4}{(r^2 + g^2)^{\frac{3}{2}}} + \alpha r \ln \frac{r}{|\alpha|} = 0. \quad (56)$$

Obviously, the radii of horizons depend on the rotation parameter a , magnetic

charge g and dark matter α . The numerical analysis of Eq. (56) suggests the possibility of two roots for a set of values of parameters, which correspond the Cauchy horizon r_- (smaller root) and the event horizon r_+ (larger root), respectively. The variation of Δ_r with respect to r for the different values of parameters a , g , and α is depicted in Figs. 5 and 6. As can be seen from Fig. 5, for any fixed parameters g and α , when $a < a_E$, the radii of Cauchy horizons increase with the increasing a while the radii of event horizons decrease with a . For $a = a_E$, these two horizons meet at r_E , that is, we have an extremal black hole with degenerate horizons. Here, the critical rotation parameter a_E and the corresponding critical radius r_E can be obtained by combining $\Delta_r = 0$ with $\partial_r \Delta_r = 0$. If $a > a_E$, Eq. (56) has no root, i.e., no horizon exists, which means there is no black hole. A similar analysis can be applied to Fig. 6. The result shows that, for any given values of parameters a and α , two horizons get closer first with the increase of g , then coincide when $g = g_E$ and eventually disappear.

Next, we further analyze the behavior of the horizons of rotating Bardeen black holes in PFD. As shown in Fig. 5, when the dark matter parameter α is fixed, for any given magnetic charge g , there always exists a critical value of a_E at which the two horizon coincide. Varying g , we thus obtained a critical curve with $M = 1$ in the parameter space (a, g) (see Fig. 7(a)), and every point on the curve corresponds to an extremal black hole with the degenerate horizons. It is worth noting that the critical curve separates the black hole region from the no black hole region. Fig. 7(a) implies that, the extremal value of the rotation parameter a_E decreases with increasing magnetic charge g . As a comparison, the critical curve of Kerr-Newman black holes is also depicted in Fig. 7(b). Actually, one can give the analytic expression of the curve, $a^2 + Q^2 = M^2$ with Q denoting the total charge of black holes. From this expression as well as Fig. 7(b), it is easily find that the critical curve is a part of circle.

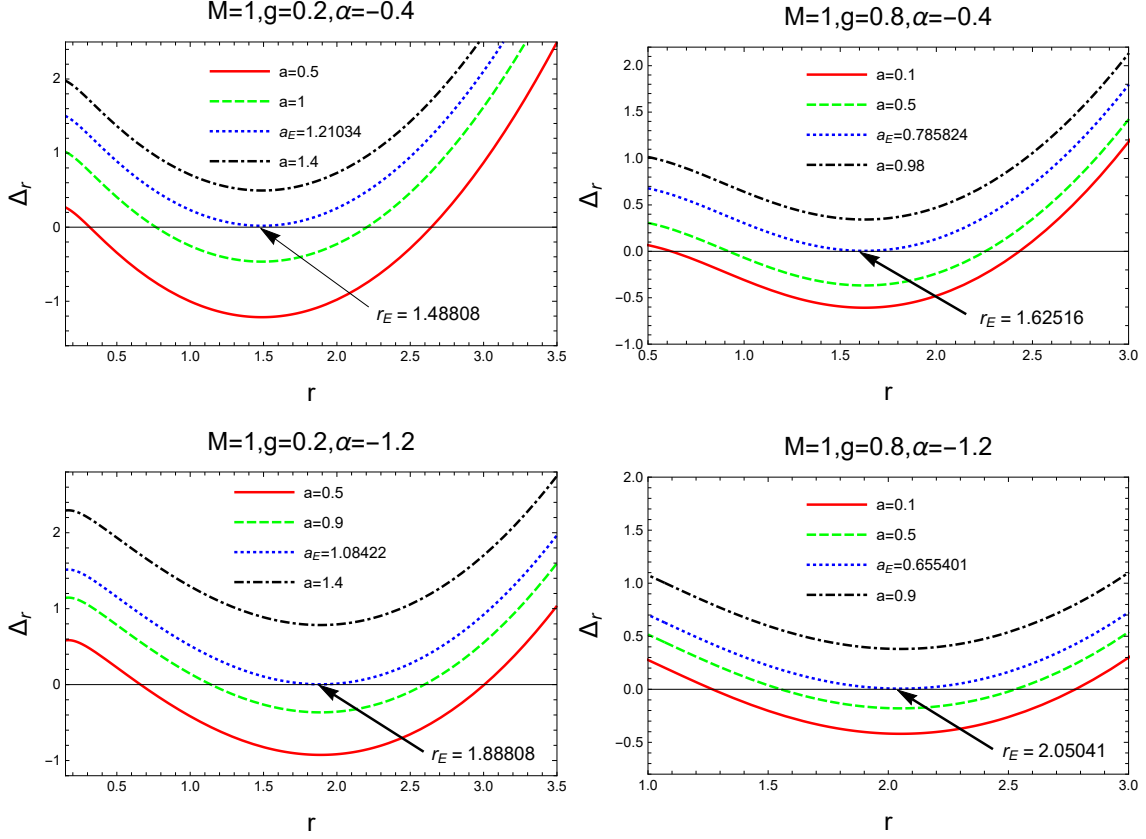


Figure 5: Plot showing the behavior of horizons vs. r for a set of fixed values of $M = 1, g$, and α by varying a .

B. Ergosphere

The ergosphere is a region bounded by the event horizon r_+ and the outer stationary limit surface (denoted by r_+^S), in fact, it lies outside the black hole. Interestingly, the ergosphere can be used to extract energy from a rotating black hole, which is known as the Penrose process [48]. We will discuss it in detail in the next section. The stationary limit surface, that is, infinite redshift surface, is a surface

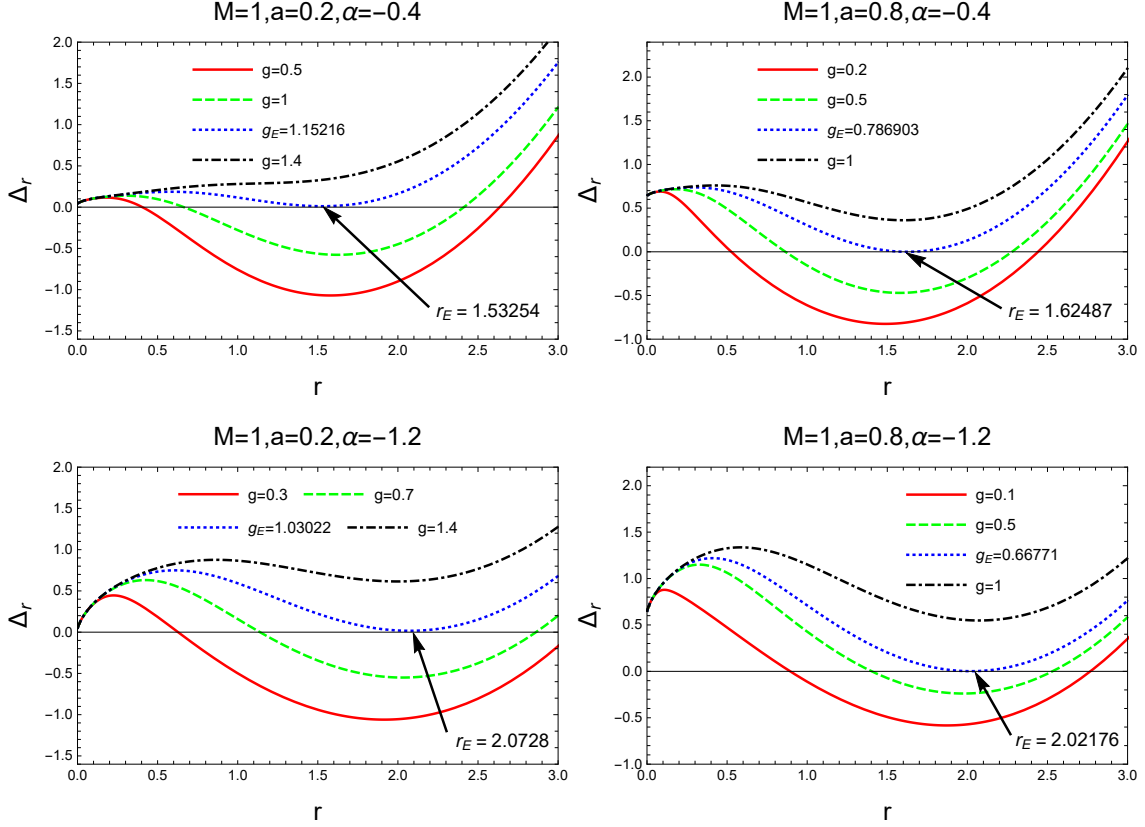
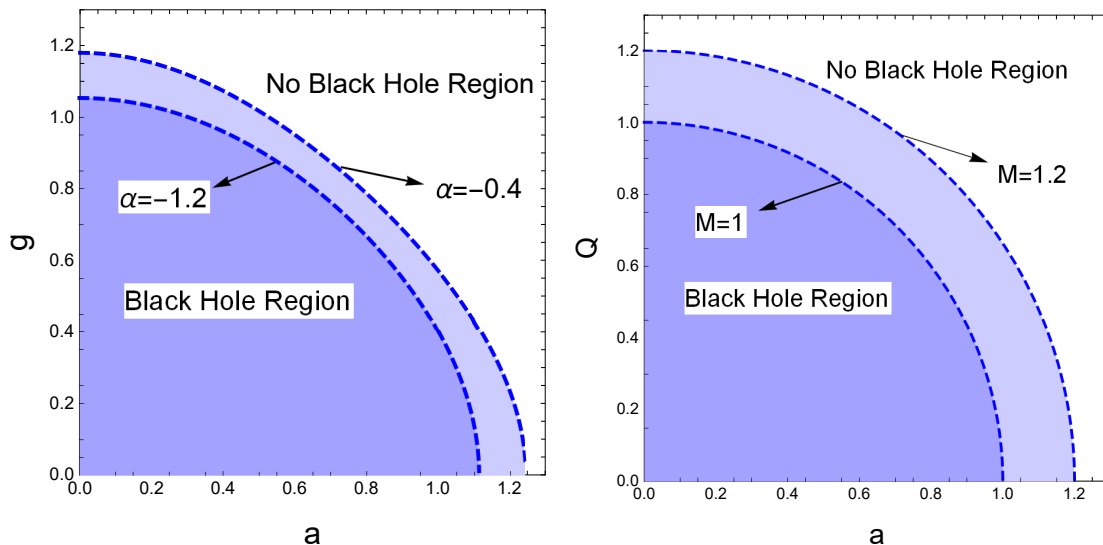


Figure 6: Plot showing the behavior of horizons vs. r for a set of fixed values of $M = 1, a,$ and α by varying g .

where the time-translation Killing vector $K^\mu = \partial_t$ satisfy $K^\mu K_\mu = 0$, or equivalently,

$$r^2 + a^2 \cos^2 \theta - \frac{2Mr^4}{(r^2 + g^2)^{\frac{3}{2}}} + \alpha r \ln \frac{r}{|\alpha|} = 0. \quad (57)$$

Solving Eq. (57) for various values of the parameters numerically, one can generally get two roots, i.e. inner stationary limit surface r_-^S and outer stationary limit surface r_+^S . Fig. 8 shows the shapes of the ergospheres and horizons for the rotating Bardeen black hole surrounded by perfect fluid dark matter. It can be seen that the size of the ergosphere increases with the rotation parameter a (see Fig. 8 horizontally) and



(a) Rotating Bardeen black hole in PFDM

(b) Kerr-Newman black hole

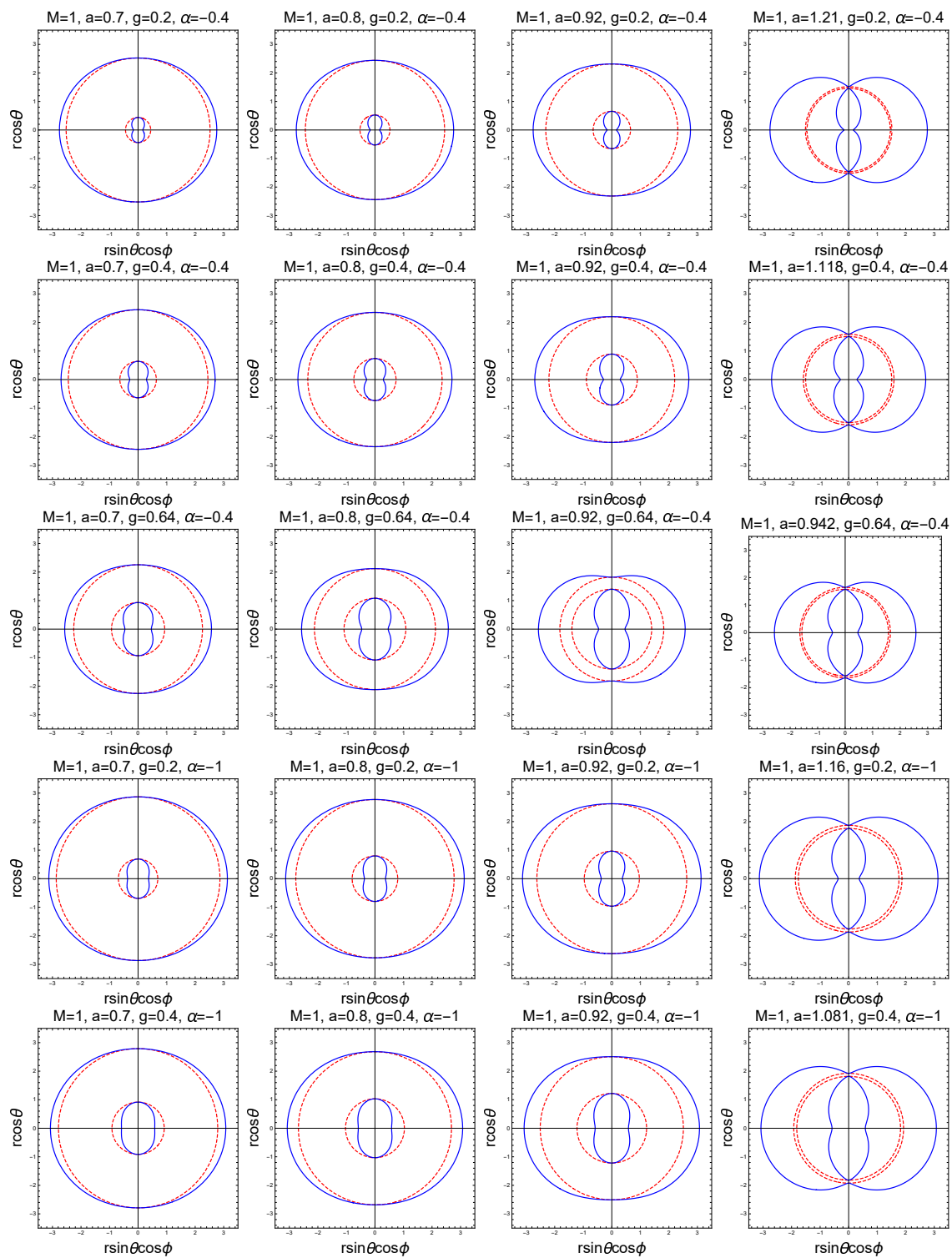
Figure 7: (a) The parameter space (a, g) for various values of $\alpha = -0.4, -1.2$.

(b) The parameter space (a, Q) for various values of $M = 1, 1.2$.

increases slightly with the increase of g (see Fig. 8 from the top down). Moreover, one can find that there exists a critical value a_E at which the inner horizon and outer horizon degenerate into one, when $a > a_E$, the ergosphere disappears.

VII. PENROSE PROCESS

Since the Killing vector $K^\mu = \partial_t$ becomes space-like inside the ergosphere, there exists the negative energy orbits. Base on this, Penrose first proposed that one can extract the rotational energy from black hole. Consider, for example, a particle A moving in the ergosphere which breaks into two particles B and C . We arrange the breakup so that the energy of the particle B falling into the black hole is negative and the particle C escape to infinity. Due to the local conservation of energy along



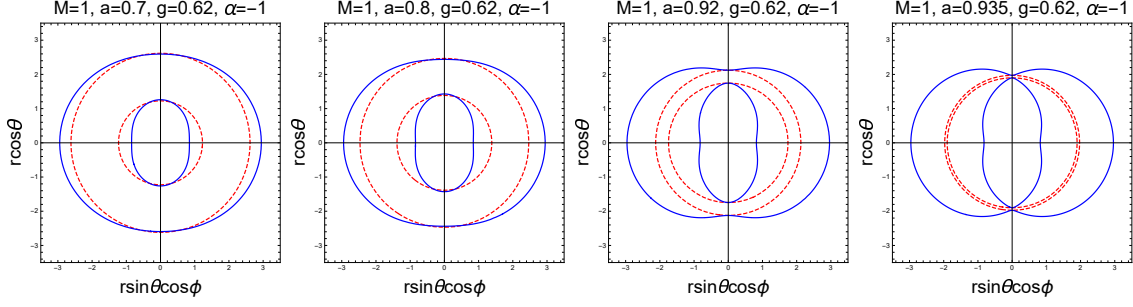


Figure 8: Illustration of the shapes of ergospheres and horizons with different value of a, g, α . The blue solid lines and red dashed lines correspond to stationary limit surfaces and horizons, respectively.

geodesics for this process, the energy of particle C will be greater than that of particle A . In order to study Penrose process quantitatively, we have followed Refs. [49–51]. For simplicity, we will restrict the motion of particles in the equatorial plane ($\theta = \frac{\pi}{2}$).

The geodesic motion for test particles in the space-time (43) are determined by the following Lagrangian

$$2\mathcal{L} = - \left(1 - \frac{2\rho}{r}\right) \dot{t}^2 - \frac{4a\rho}{r} \dot{t}\dot{\phi} + \frac{r^2}{\Delta_r} \dot{r}^2 + \left(r^2 + a^2 + \frac{2a^2\rho}{r}\right) \dot{\phi}^2, \quad (58)$$

where $2\rho = \frac{2Mr^3}{(r^2+g^2)^{\frac{3}{2}}} - \alpha \ln \frac{r}{|\alpha|}$ and $\Delta_r = r^2 + a^2 - \frac{2Mr^4}{(r^2+g^2)^{\frac{3}{2}}} + \alpha r \ln \frac{r}{|\alpha|}$. In terms of the Euler-Lagrange equation, one gets two conserved quantities, i.e. the energy E and the angular momentum L of the test particle:

$$E \equiv -\frac{\partial \mathcal{L}}{\partial \dot{t}} = -g_{tt}\dot{t} - g_{t\phi}\dot{\phi} \quad \text{and} \quad L \equiv \frac{\partial \mathcal{L}}{\partial \dot{\phi}} = g_{t\phi}\dot{t} + g_{\phi\phi}\dot{\phi}, \quad (59)$$

where the dot (\cdot) denotes derivatives with respect to affine parameter λ .

The radial equation for the geodesic motion of a test particle can be obtained by means of Eqs. (58) and (59) as

$$r^4 \dot{r}^2 = E^2 (r^4 + a^4 + a^2(2r^2 - \Delta_r)) + L^2(a^2 - \Delta_r) - 4aLE\rho r + \delta r^2 \Delta_r, \quad (60)$$

where $\delta = -1, 0, 1$ correspond to time-like, null and space-like geodesic respectively. Suppose that the breakup happened at the turning point of the geodesic, where $\dot{r} = 0$, then from the radial equation for equatorial geodesic it follows that

$$E = \frac{2a\rho r L \pm r\sqrt{\Delta_r}\sqrt{L^2 r^2 - \delta(r^4 + a^4 + a^2(2r^2 - \Delta_r))}}{r^4 + a^4 + a^2(2r^2 - \Delta_r)}, \quad (61)$$

and

$$L = \frac{-2a\rho r E \pm r\sqrt{\Delta_r}\sqrt{E^2 r^2 + \delta(r^2 - 2\rho r)}}{\Delta_r - a^2}. \quad (62)$$

Using Eq. (61), one could derive the condition while the value of the energy is negative: in order to have positive energy in the limit $a \rightarrow 0$, we must retain only the positive sign; on the other hand when $a \neq 0$, a necessary criterion for having negative energy is $L < 0$. Thus in order to have negative energy, we must also have

$$4a^2 \rho^2 r^2 L^2 > r^2 \Delta_r [L^2 r^2 - \delta(r^4 + a^4 + a^2(2r^2 - \Delta_r))],$$

or alternatively

$$1 - \frac{2\rho}{r} < \delta \frac{\Delta_r}{L^2}. \quad (63)$$

Since $g_{tt}(\theta = \frac{\pi}{2}) = -(1 - \frac{2\rho}{r})$, the above inequality clearly suggests that this can happen in the ergosphere.

Let us now consider a massive particle ($\delta = -1$) with $E_A = 1 > 0$ (without loss of generality) and angular momentum L_A entering the ergosphere. This particle then decays into two photons ($\delta = 0$) with energies and angular momenta (E_B, L_B) and (E_C, L_C) respectively. We could arrange this process such that the photon which falls into the event horizon has negative energy and the photon which escapes to

infinity has positive energy. From Eq. (62), we have

$$\begin{aligned} L_A &= \frac{-2a\rho r + r\sqrt{\Delta_r}\sqrt{2\rho r}}{\Delta_r - a^2} = \alpha_A, \\ L_B &= \frac{-2a\rho r - r^2\sqrt{\Delta_r}}{\Delta_r - a^2} E_B = \alpha_B(r)E_B, \\ L_C &= \frac{-2a\rho r + r^2\sqrt{\Delta_r}}{\Delta_r - a^2} E_C = \alpha_C(r)E_C. \end{aligned} \quad (64)$$

The conservation of energy and angular momentum gives

$$E_B + E_C = E_A = 1 \quad (65)$$

and

$$L_B + L_C = \alpha_B(r)E_B + \alpha_C(r)E_C = L_A = \alpha_A(r). \quad (66)$$

Solving Eqs. (65) and (66) and using Eq. (64), one finally gets

$$E_B = \frac{1}{2} \left(1 - \sqrt{1 + \frac{a^2 - \Delta_r}{r^2}} \right) = \frac{1}{2} \left(1 - \sqrt{\frac{2Mr^2}{(r^2 + g^2)^{\frac{3}{2}}} - \frac{\alpha}{r} \ln \frac{r}{|\alpha|}} \right), \quad (67)$$

$$E_C = \frac{1}{2} \left(1 + \sqrt{1 + \frac{a^2 - \Delta_r}{r^2}} \right) = \frac{1}{2} \left(1 + \sqrt{\frac{2Mr^2}{(r^2 + g^2)^{\frac{3}{2}}} - \frac{\alpha}{r} \ln \frac{r}{|\alpha|}} \right). \quad (68)$$

Clearly, the photon C that escapes from the black hole to infinity has more energy than the initial particle A , and the energy gain ΔE in this process is

$$\Delta E = \frac{1}{2} \left(\sqrt{\frac{2Mr^2}{(r^2 + g^2)^{\frac{3}{2}}} - \frac{\alpha}{r} \ln \frac{r}{|\alpha|}} - 1 \right) = -E_B. \quad (69)$$

It follows from Eq. (67) that the maximum gain in energy occurs at the event horizon, $\Delta_r = 0$ and the maximal efficiency of Penrose process is then given by

$$E_{ffmax} = \frac{E_A + \Delta E}{E_A} = \frac{1}{2} \left(1 + \sqrt{\frac{2Mr_+^2}{(r_+^2 + g^2)^{\frac{3}{2}}} - \frac{\alpha}{r_+} \ln \frac{r_+}{|\alpha|}} \right), \quad (70)$$

which can be shown visually in Fig. 9. It is easy to see that the maximal efficiency E_{ffmax} increases with the increase of spin parameter a and magnetic parameter g .

Interestingly, the effect of dark matter parameter α on E_{ffmax} is nonmonotonic. When $\alpha > \alpha^C$ (critical value), the maximal efficiency E_{ffmax} decrease with its decrease; however, when $\alpha < \alpha^C$, E_{ffmax} increases with its decrease. In fact, this is caused by the influence of α on the event horizon.

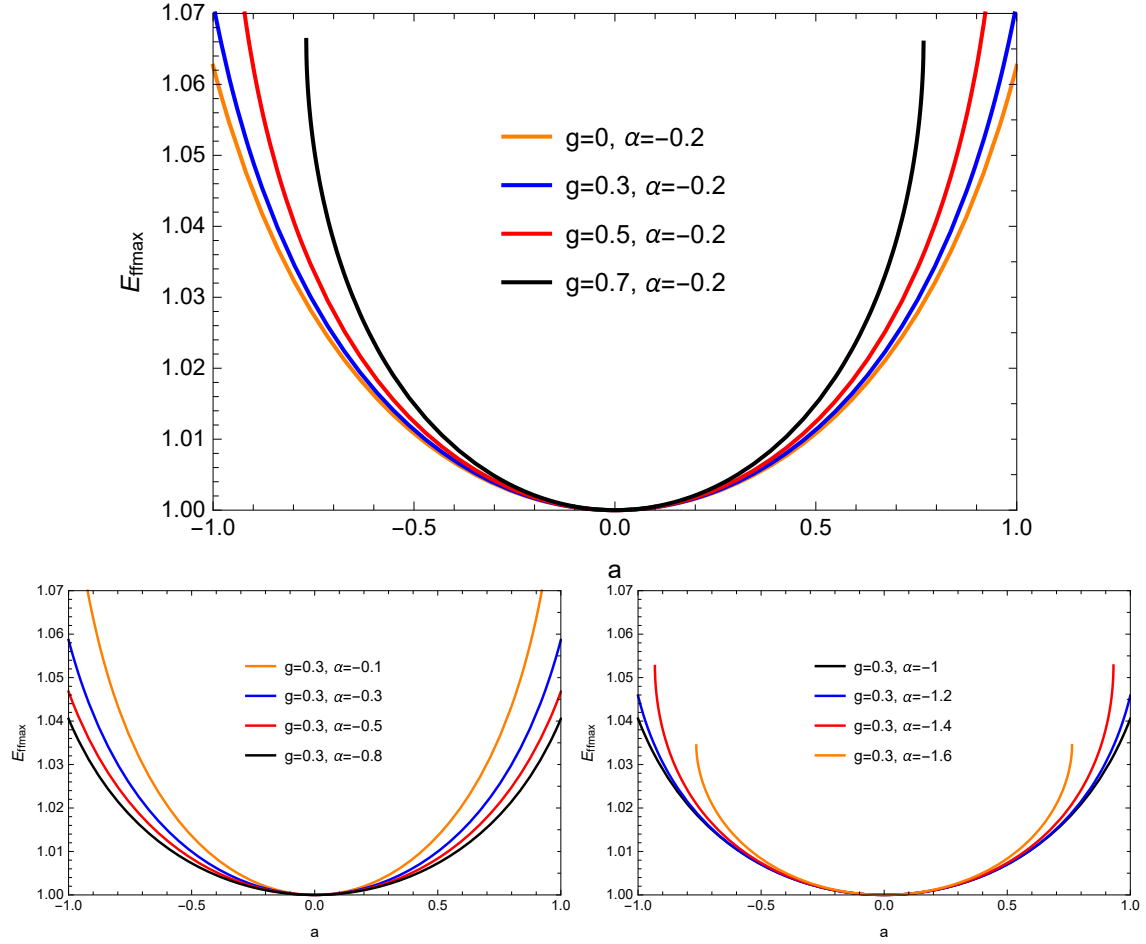


Figure 9: Variation of maximal efficiency of Penrose process with a , g and α .

VIII. CONCLUSIONS AND DISCUSSIONS

In this paper, we have obtained the exact solution of the static spherically symmetric Bardeen black hole surrounded by perfect fluid dark matter and then studied the thermodynamic properties. We first derived the thermodynamic first law and the corresponding Smarr formula by treating the magnetic charge g and dark matter parameter α as thermodynamic variables. Furthermore, we discussed the thermodynamic stability of the black hole by means of heat capacity. The result showed that, there exists a critical radius r_+^C , where the heat capacity diverges and the second order phase transition occurs. The critical radius r_+^C increases with the magnetic charge g and decreases with the dark matter parameter α .

With the Newman-Janis algorithm, we generalized the static spherically symmetric Bardeen black hole surrounded by PFDM to the corresponding rotating solution. According to the components of the energy-momentum tensor, we found that the weak energy condition is violated near the origin of the rotating Bardeen black holes surrounded by PFDM, which happens for all the rotating regular black holes. Meanwhile, we constrained the dark matter parameter to $\alpha < 0$ in terms of the weak energy condition.

The structure of the black hole horizons was studied in detail. By solving the relevant equation numerically, we found that for any fixed parameters g and α , when $a < a_E$, the radii of Cauchy horizons increase with the increasing a while the radii of event horizons decrease with a . For $a = a_E$, we have an extremal black hole with degenerate horizons. If $a > a_E$, no black hole will form. Similarly, for any given values of parameters a and α , two horizons get closer first with the increase of g , then coincide when $g = g_E$ and eventually disappear. Furthermore, for a fixed dark matter parameter α , we can obtain a critical curve in the parameter space (a, g) , which separates the black hole region from the no black hole region. We found

that the extremal value of the rotation parameter a_E decreases with the magnetic charge parameter g . By the analysis to ergospheres, we have seen that the size of the ergosphere increases with the rotation parameter a and increases slightly with the increase of g . Moreover, when $a > a_E$, we have no ergosphere.

Finally, the energy extraction was discussed by taking into the Penrose process in rotating Bardeen black hole surrounded by PFDM. We have demonstrated that the maximal efficiency E_{ffmax} increases with the increase of spin parameter a and magnetic parameter g . However, the effect of dark matter parameter α on E_{ffmax} is nonmonotonic, which is caused by the influence of α on the event horizon.

Very recently, first image of the M87* black hole was obtained using the sub-millimeter “Event Horizon Telescope” based on the very-long baseline interferometry [52]. The observation to black hole shadows will be a useful tool for a better understanding of astrophysical black holes and for testing the modified gravity models as well. Hence, as done in Refs. [53–55], we intend to further constrain the relevant black hole parameters by studying the optical properties of the Bardeen black holes surrounded by perfect fluid dark matter.

CONFLICTS OF INTEREST

The authors declare that there are no conflicts of interest regarding the publication of this paper.

ACKNOWLEDGMENTS

We would like to thank the National Natural Science Foundation of China (Grant No.11571342) for supporting us on this work. This work makes use of the Black Hole Perturbation Toolkit.

REFERENCES

- [1] Stephen W Hawking and George Francis Rayner Ellis. *The large scale structure of space-time*, volume 1. Cambridge University Press, 1973.
- [2] Stephen Hawking and Roger Penrose. *The nature of space and time*. Princeton University Press, 2010.
- [3] James M Bardeen. Non-singular general-relativistic gravitational collapse. In *Proc. Int. Conf. GR5, Tbilisi*, volume 174, 1968.
- [4] Eloy Ayón-Beato and Alberto Garcia. The Bardeen model as a nonlinear magnetic monopole. *Physics Letters B*, 493(1-2):149–152, 2000.
- [5] Eloy Ayon-Beato and Alberto Garcia. Regular black hole in general relativity coupled to nonlinear electrodynamics. *Physical Review Letters*, 80(23):5056, 1998.
- [6] Sean A Hayward. Formation and evaporation of nonsingular black holes. *Physical Review Letters*, 96(3):031103, 2006.
- [7] Waldemar Berej, Jerzy Matyjasek, Dariusz Tryniecki, and Mariusz Woronowicz. Regular black holes in quadratic gravity. *General Relativity and Gravitation*, 38(5):885–906, 2006.
- [8] Andrei D Sakharov. The initial stage of an expanding universe and the appearance of a nonuniform distribution of matter. *Sov. Phys. JETP*, 22:241–249, 1966.
- [9] Cao H Nam. On non-linear magnetic-charged black hole surrounded by quintessence. *General Relativity and Gravitation*, 50(6):57, 2018.
- [10] Cosimo Bambi and Leonardo Modesto. Rotating regular black holes. *Physics Letters B*, 721(4-5):329–334, 2013.

- [11] Juliano CS Neves and Alberto Saa. Regular rotating black holes and the weak energy condition. *Physics Letters B*, 734:44–48, 2014.
- [12] Rahul Kumar, Sushant G Ghosh, and Anzhong Wang. Shadow cast and deflection of light by charged rotating regular black holes. *Physical Review D*, 100(12):124024, 2019.
- [13] Sushant G Ghosh, Muhammed Amir, and Sunil D Maharaj. Ergosphere and shadow of a rotating regular black hole. *Nuclear Physics B*, page 115088, 2020.
- [14] Peter AR Ade, N Aghanim, M Arnaud, Mark Ashdown, J Aumont, C Baccigalupi, AJ Banday, RB Barreiro, JG Bartlett, N Bartolo, et al. Planck 2015 results-xiii. cosmological parameters. *Astronomy and Astrophysics*, 594:A13, 2016.
- [15] VV Kiselev. Quintessence and black holes. *Classical and Quantum Gravity*, 20(6):1187, 2003.
- [16] Bobir Toshmatov, Zdeněk Stuchlík, and Bobomurat Ahmedov. Rotating black hole solutions with quintessential energy. *The European Physical Journal Plus*, 132(2):1–21, 2017.
- [17] Mahamat Saleh, Bouetou Bouetou Thomas, and Timoleon Crepin Kofane. Thermodynamics and phase transition from regular Bardeen black hole surrounded by quintessence. *International Journal of Theoretical Physics*, 57(9):2640–2647, 2018.
- [18] Carlos A Benavides-Gallego, Ahmadjon Abdujabbarov, and Cosimo Bambi. Rotating and nonlinear magnetic-charged black hole surrounded by quintessence. *Physical Review D*, 101(4):044038, 2020.
- [19] Sushant G Ghosh, Sunil D Maharaj, Dharmanand Baboolal, and Tae-Hun Lee. Lovelock black holes surrounded by quintessence. *The European Physical Journal C*, 78(2):1–8, 2018.
- [20] Yu Zhang and YX Gui. Quasinormal modes of gravitational perturbation around a Schwarzschild black hole surrounded by quintessence. *Classical and Quantum Gravity*,

23(22):6141, 2006.

- [21] Sushant G Ghosh. Rotating black hole and quintessence. *The European Physical Journal C*, 76(4):222, 2016.
- [22] Songbai Chen, Bin Wang, and Rukeng Su. Hawking radiation in a d-dimensional static spherically symmetric black hole surrounded by quintessence. *Physical Review D*, 77(12):124011, 2008.
- [23] Ahmadjon Abdujabbarov, Bobir Toshmatov, Zdeněk Stuchlík, and Bobomurat Ahmedov. Shadow of the rotating black hole with quintessential energy in the presence of plasma. *International Journal of Modern Physics D*, 26(06):1750051, 2017.
- [24] Mustapha Azreg-Aïnou and Manuel E Rodrigues. Thermodynamical, geometrical and Poincaré methods for charged black holes in presence of quintessence. *Journal of High Energy Physics*, 2013(9):146, 2013.
- [25] VV Kiselev. Quintessential solution of dark matter rotation curves and its simulation by extra dimensions. *arXiv:gr-qc/0303031*, 2003.
- [26] Ming-Hsun Li and Kwei-Chou Yang. Galactic dark matter in the phantom field. *Physical Review D*, 86(12):123015, 2012.
- [27] Sumarna Haroon, Mubasher Jamil, Kimet Jusufi, Kai Lin, and Robert B Mann. Shadow and deflection angle of rotating black holes in perfect fluid dark matter with a cosmological constant. *Physical Review D*, 99(4):044015, 2019.
- [28] Xian Hou, Zhaoyi Xu, and Jiancheng Wang. Rotating black hole shadow in perfect fluid dark matter. *Journal of Cosmology and Astroparticle Physics*, 2018(12):040, 2018.
- [29] Zhaoyi Xu, Xian Hou, and Jiancheng Wang. Kerr–anti-de Sitter/de Sitter black hole in perfect fluid dark matter background. *Classical and Quantum Gravity*, 35(11):115003, 2018.

- [30] Zhaoyi Xu, Xian Hou, Xiaobo Gong, and Jiancheng Wang. Kerr–Newman-AdS black hole surrounded by perfect fluid matter in Rastall gravity. *The European Physical Journal C*, 78(6):513, 2018.
- [31] Muhammad Rizwan, Mubasher Jamil, and Kimet Jusufi. Distinguishing a Kerr-like black hole and a naked singularity in perfect fluid dark matter via precession frequencies. *Physical Review D*, 99(2):024050, 2019.
- [32] Leonardo Balart and Sharmanthie Fernando. A Smarr formula for charged black holes in nonlinear electrodynamics. *Modern Physics Letters A*, 32(39):1750219, 2017.
- [33] Rong-Gen Cai, Li-Ming Cao, Li Li, and Run-Qiu Yang. P-V criticality in the extended phase space of Gauss-Bonnet black holes in AdS space. *Journal of High Energy Physics*, 2013(9):5, 2013.
- [34] Zhaoyi Xu, Xian Hou, Jiancheng Wang, and Yi Liao. Perfect fluid dark matter influence on thermodynamics and phase transition for a Reissner-Nordstrom-anti-de Sitter black hole. *Advances in High Energy Physics*, 2019, 2019.
- [35] Shao-Wen Wei and Yu-Xiao Liu. Extended thermodynamics and microstructures of four-dimensional charged Gauss-Bonnet black hole in AdS space. *Physical Review D*, 101(10):104018, 2020.
- [36] Ezra T Newman and AI Janis. Note on the Kerr spinning-particle metric. *Journal of Mathematical Physics*, 6(6):915–917, 1965.
- [37] Bobir Toshmatov, Zdeněk Stuchlík, and Bobomurat Ahmedov. Generic rotating regular black holes in general relativity coupled to nonlinear electrodynamics. *Physical Review D*, 95(8):084037, 2017.
- [38] Rahul Kumar and Sushant G Ghosh. Rotating black hole in Rastall theory. *The European Physical Journal C*, 78(9):750, 2018.
- [39] Zhaoyi Xu and Jiancheng Wang. Kerr-Newman-AdS black hole in quintessential dark energy. *Physical Review D*, 95(6):064015, 2017.

- [40] Zhaoyi Xu, Xiaobo Gong, and Shuang-Nan Zhang. Black hole immersed dark matter halo. *Physical Review D*, 101(2):024029, 2020.
- [41] Rajibul Shaikh. Black hole shadow in a general rotating spacetime obtained through Newman-Janis algorithm. *Physical Review D*, 100(2):024028, 2019.
- [42] Hyeong-Chan Kim, Bum-Hoon Lee, Wonwoo Lee, and Youngone Lee. Rotating black holes with an anisotropic matter field. *Physical Review D*, 101(6):064067, 2020.
- [43] Kimet Jusufi, Mubasher Jamil, Hrishikesh Chakrabarty, Qiang Wu, Cosimo Bambi, and Anzhong Wang. Rotating regular black holes in conformal massive gravity. *Physical Review D*, 101(4):044035, 2020.
- [44] Mustapha Azreg-Aïnou, Sumarna Haroon, Mubasher Jamil, and Muhammad Rizwan. Rotating normal and phantom Einstein-Maxwell-dilaton black holes: Geodesic analysis. *International Journal of Modern Physics D*, 28(04):1950063, 2019.
- [45] Cheng Liu, Tao Zhu, Qiang Wu, Kimet Jusufi, Mubasher Jamil, Mustapha Azreg-Aïnou, and Anzhong Wang. Shadow and quasinormal modes of a rotating loop quantum black hole. *Physical Review D*, 101(8):084001, 2020.
- [46] Mustapha Azreg-Aïnou. Generating rotating regular black hole solutions without complexification. *Physical Review D*, 90(6):064041, 2014.
- [47] Mustapha Azreg-Aïnou. From static to rotating to conformal static solutions: rotating imperfect fluid wormholes with (out) electric or magnetic field. *The European Physical Journal C*, 74(5):2865, 2014.
- [48] Robert M Wald. *General Relativity*. University of Chicago Press, 2010.
- [49] Sumarna Haroon, Mubasher Jamil, Kai Lin, Petar Pavlovic, Marko Sossich, and Anzhong Wang. The effects of running gravitational coupling on rotating black holes. *The European Physical Journal C*, 78(6):519, 2018.
- [50] Parthapratim Pradhan. Study of energy extraction and epicyclic frequencies in Kerr-MOG (modified gravity) black hole. *The European Physical Journal C*, 79(5):1–16,

2019.

- [51] Sourav Bhattacharya. Kerr-de Sitter spacetime, Penrose process, and the generalized area theorem. *Physical Review D*, 97(8):084049, 2018.
- [52] Kazunori Akiyama, Antxon Alberdi, Walter Alef, Keiichi Asada, Rebecca Azulay, Anne-Kathrin Baczko, David Ball, Mislav Baloković, John Barrett, Dan Bintley, et al. First M87 event horizon telescope results. IV. Imaging the central supermassive black hole. *The Astrophysical Journal Letters*, 875(1):L4, 2019.
- [53] Zdenek Stuchlík and Jan Schee. Shadow of the regular Bardeen black holes and comparison of the motion of photons and neutrinos. *The European Physical Journal C*, 79(1):1–13, 2019.
- [54] Peng-Zhang He, Qi-Qi Fan, Hao-Ran Zhang, and Jian-Bo Deng. Shadows of rotating Hayward-de Sitter black holes with astrometric observables. *The European Physical Journal C*, 80(12):1–13, 2020.
- [55] He-Xu Zhang, Cong Li, Peng-Zhang He, Qi-Qi Fan, and Jian-Bo Deng. Optical properties of a Brane-World black hole as photons couple to the Weyl tensor. *European Physical Journal C*, 80(5):1–11, 2020.